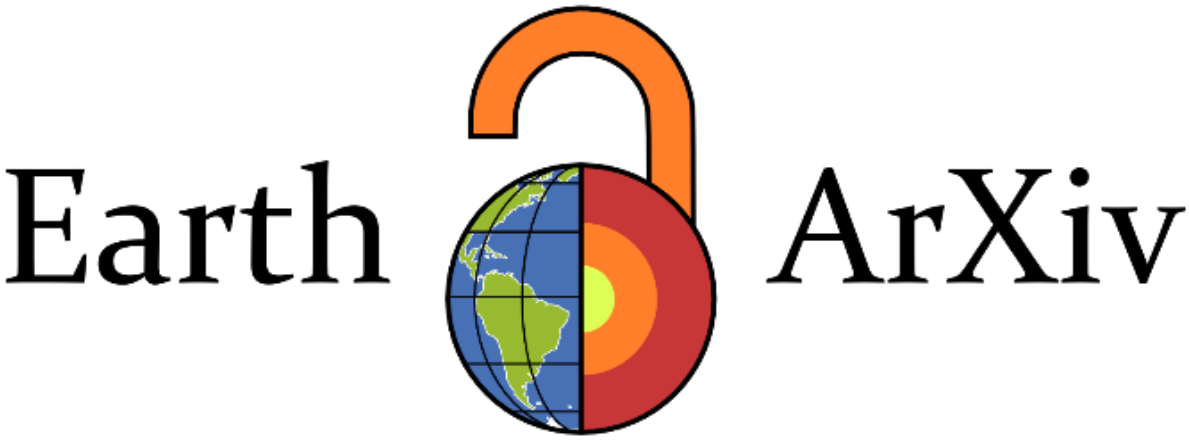

Continuous Water Surface Elevation Estimates Using Deep Learning with Legacy Altimetry and Surface Water and Ocean Topography Data

Chinmay Deval[1,2,*], Alqamah Sayeed[1,2], Ashutosh Limaye[2]

[1.] Earth System Science Center, University of Alabama in Huntsville, Huntsville, AL, United States of America
[2.] NASA Marshall Space Flight Center, Huntsville, AL, United States of America
[*]corresponding author(s): Chinmay Deval (chinmay.deval@uah.edu)

Abstract

We present the development of a high-temporal-resolution global dataset of daily river water surface elevation (WSE), spanning January 2008 through May 2025. By utilizing a deep learning framework to integrate legacy satellite altimetry and the Surface Water and Ocean Topography (SWOT) mission data, we produced a continuous record covering 9,184 river reaches, 5,926 rivers, and 1,342 basins. The densification process successfully reconciles the sparse temporal sampling of missions such as Jason and Sentinel with the spatial precision of the SWOT Ka-band interferometer. Evaluation metrics demonstrate robust performance, with a median correlation (R) of 0.46 against Hydroweb calibration data and a superior median R of 0.62 against independent SWOT observations. Spatial analysis confirms that the model maintains near zero global median bias relative to legacy data. This multidecadal resource provides a critical analytical foundation for global monitoring and the management of freshwater resources under varying climatic zones. Ultimately, this dataset bridges the strategic gap between sparse legacy altimetry observations and the high-resolution capabilities of the contemporary SWOT mission.

Background & Summary

River water surface elevation (WSE) is a foundational hydrological state variable that governs the hydraulic gradients, connectivity, and energy dynamics of terrestrial water systems. At continental and global scales, the ability to monitor WSE continuously is essential for characterizing the storage and flux of surface water, including for applications like flood early warning systems, assessment of freshwater availability, and the calibration and validation of hydrological and hydraulic models, across diverse landscapes. Yet in-situ river gauge networks which have historically been an accurate source of WSE records, are spatially sparse, unevenly distributed, and have suffered a steady decline in density across many regions of the world[1,2]. Observational coverage remains particularly deficient across remote tropical, boreal, and arid catchments, which are simultaneously among the most hydrologically vulnerable regions to anthropogenic and climatic disruptions.

Over recent decades, satellite altimetry has emerged as an indispensable complement to ground based monitoring. Legacy radar altimetry missions, including the TOPEX/Poseidon, Jason-1, Jason-2, Jason-3, and Sentinel-6 Michael Freilich series as well as the Envisat, ERS-2, and SARAL/AltiKa instruments, have accumulated multi-decadal observational records. These missions employ along-track nadir pointing altimeters with ground track repeat periods of approximately 10 to 35 days, providing intermittent WSE estimates at fixed virtual station locations where satellite tracks cross water surfaces. The Hydroweb database[3] consolidates these multi-mission observations into harmonized long-term WSE time series at thousands of virtual stations worldwide, forming one of the most comprehensive legacy altimetry archives available to the global hydrology community. While sufficient for capturing seasonal or inter-

annual trends, their coarse temporal sampling leaves the vast majority of calendar days unobserved. Consequently, these records are systematically unable to resolve sub-monthly hydrologic dynamics, rapid recession limbs, or the daily-scale variability required for monitoring and decision making.

The launch of the Surface Water and Ocean Topography (SWOT) mission in December 2022 represents a fundamental breakthrough in the remote sensing of terrestrial water surfaces[4]. Equipped with the Ka-band Radar Interferometer (KaRIn), SWOT provides simultaneous two-dimensional measurements of WSE, width, and slope across a 120-km wide swath. Its unprecedented spatial resolution allows it to observe the global river network on a consistent topological baseline, precisely aligning with the SWORD reach database[5]. Post-launch validation has confirmed SWOT's extraordinary spatial fidelity, demonstrating centimeter-to-decimeter accuracy in previously ungauged, complex river systems[6–9], and even proving capable of detecting fine-scale lateral water-surface superelevation in meandering river bends[10]. Furthermore, by simultaneously providing river width and slope, SWOT has enabled the first global estimates of river discharge without reliance on in-situ gauge data[11].

While SWOT provides massive spatial detail, producing roughly 8 terabytes of continental water data daily[12], its nominal 21-day repeat orbit remains insufficient to capture the rapid dynamics of transient hydrological events, such as flash floods, on its own[13]. To address this temporal gap, the hydrological community has increasingly relied on computational models acting as "dynamical interpolators"[12]. Recent efforts have employed complex data assimilation (DA) frameworks using SWOT altimetry to generate continuous discharge and refine hydraulic parameters for flood reanalysis[14–17]. Other approaches have utilized reach-based linear regressions across neighbouring multi-mission altimetry tracks to estimate daily WSE[13].

The dataset described in this paper directly addresses this observational and computational gap. We present a globally consistent, temporally continuous daily WSE dataset covering 9,184 river reaches across all major continental basins from January 2008 to May 2025. By applying a deep learning framework, we temporally densify the historical record by integrating the legacy altimetry archive (Hydroweb) with continuous daily meteorological and hydrological forcing from the Global Land Data Assimilation System (GLDAS; Rodell et al., 2004) and static catchment morphology from RiverAtlas[18]. Critically, this dataset is independently validated against SWOT WSE measurements at the co-located SWOT node. The densified estimates reproduce observed WSE variability with acceptable accuracy across a broad range of river types and hydroclimatic regimes. Figure 1 illustrates an example time series for a representative reach, showing the agreement among the model output, Hydroweb observations, and SWOT measurements at a site on the Amazon River basin.

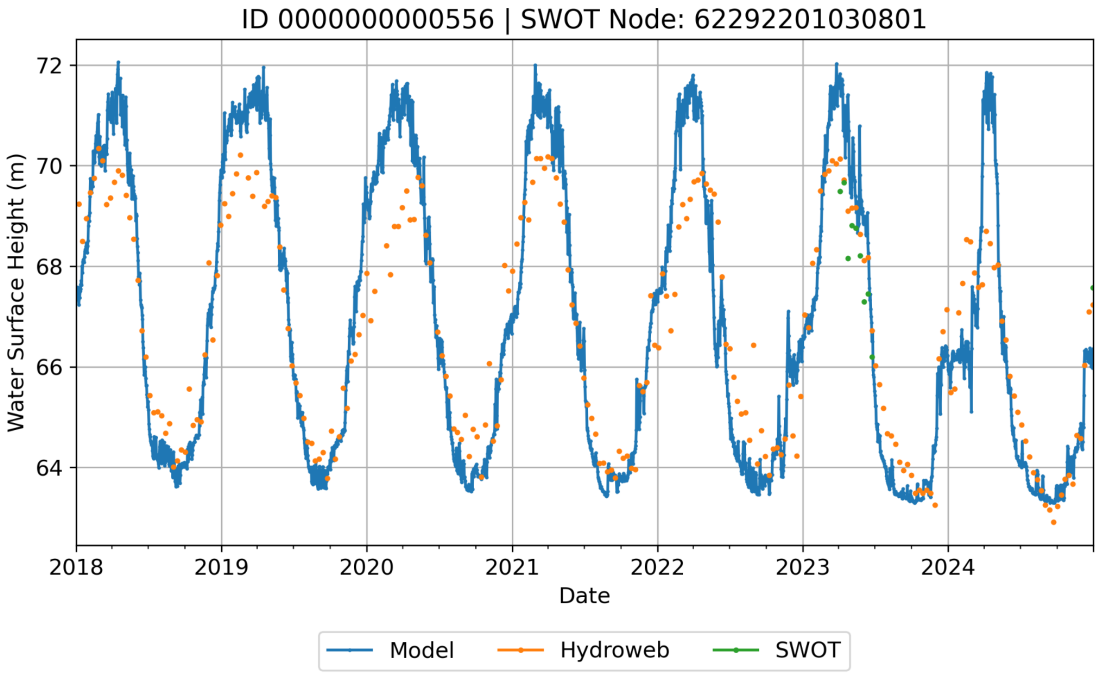

Figure 1: Example daily water surface elevation (WSE) time series for reach ID 0000000000556 / SWOT node 62292201030801. The continuous blue line represents the deep learning model output; orange points are Hydroweb virtual station observations used for training and calibration; green points are independent SWOT observations used for validation. The seasonal hydrological cycle with a peak-to-trough amplitude of approximately 8 m is well reproduced by the model over the 2018-2024 period.

The primary applications of this dataset include: (1) Water level monitoring and early warning through the provision of continuous antecedent WSE conditions that complement the episodic, high-precision observations of SWOT; (2) assessment of inter-annual and decadal trends in river water levels associated with climate variability and human water use; and (3) pre-SWOT gap-filling and temporal densification of the SWOT observational record, extending continuous WSE coverage back to 2008; among many others..

Methods

To ensure the reproducibility of the neural network predictions, a standardized production pipeline was implemented. This approach bridges the gap between disparate satellite altimetry sources, land-surface model outputs, and catchment morphology data to produce a gap-filled daily WSE time series at global scale.

Data Source Integration

The spatial backbone of the dataset is the SWORD reach network (version 16; Altenau et al., 2021), which delineates river reaches globally for rivers with widths exceeding approximately 30 m. SWORD reach centroids were co-located with Hydroweb virtual gauge locations by identifying the nearest gauge within a maximum search radius, enabling the integration of WSE records from the following legacy altimetry missions: ERS-2 and ENVISAT, SARAL/AltiKa, Jason-1, Jason-2, and Jason-3, and Sentinel-3A.

This co-location process yielded 9,184 qualifying river reaches for which both a Hydroweb WSE record, SWOT node WSE record, and GLDAS forcing data were available over the target period

(January 2008 to May 2025). Figure 2 illustrates the global distribution of observation density for the Hydroweb and SWOT networks for the target period.

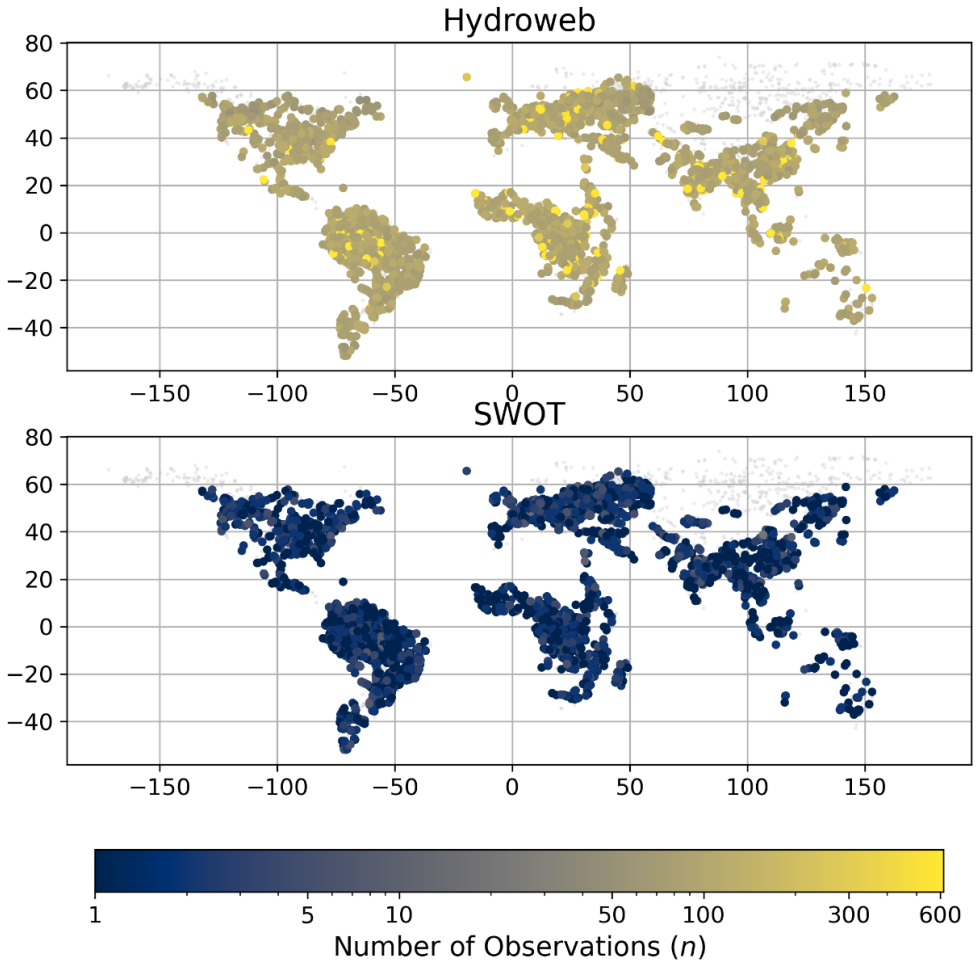

Figure 2: Global distribution of the number of observations (n) per virtual station for Hydroweb (top) and SWOT (bottom). Hydroweb station density (yellow-brown color scale) reflects the multi-decadal accumulation of legacy altimetry observations.

Predictor Selection and Normalization

The model utilizes a comprehensive set of meteorological, hydrological, and geomorphological predictors drawn from two supplementary data sources: the Global Land Data Assimilation System (GLDAS[19]) and the RiverAtlas database[18]. GLDAS provides daily gridded estimates of land-surface state and flux variables at 0.25° spatial resolution. RiverAtlas supplies static reach-level morphological and catchment attributes derived from HydroSHEDS. Table 1 summarizes the full predictor taxonomy.

Table 1: Predictor taxonomy for the deep learning framework, categorized by source dataset.

Category	Variable	Description
Meteorological & Hydrological (GLDAS)	AvgSurfT_tavg	Average surface temperature
	Evap_tavg	Evapotranspiration

	TWS_tavg	Terrestrial water storage
	GWS_tavg	Groundwater storage
	SoilMoist_P_tavg	Soil moisture
	Qs_tavg	Surface runoff / discharge
	Qsb_tavg	Subsurface baseflow
Catchment & Geomorphological (RiverAtlas)	CATCH_SKM	Catchment area (km²)
	DIST_DN_KM	Distance downstream (km)
	DIST_UP_KM	Distance upstream (km)
	ENDORHEIC	Endorheic basin indicator (binary)
	MEAN_ALTITUDE	Mean altitude of the reach
	ORD_CLAS	Stream order class
	ORD_FLOW	Flow direction order
	ORD_STRA	Strahler stream order
	UPLAND_SKM	Upland drainage area (km²)
Derived	SED	Sun-Earth Distance (Proxy for seasonality)

All predictors undergo station-specific normalization to a 0–1 range prior to model training. This step is essential to prevent larger river systems with high absolute WSE magnitudes from dominating the neural network weights over smaller tributaries, ensuring that the model learns globally applicable WSE-predictor relationships rather than reach-specific offsets.
The target variable is the station-specific normalized WSE, defined as:

$$\text{Target} = \text{ORTHOMETRIC\_HEIGHT\_M} - \text{min\_ortho\_height}$$

where min_ortho_height is the historical minimum orthometric elevation recorded at each individual Hydroweb station over the full observational period. By subtracting the station-specific minimum, the network is trained to predict WSE variance (hydrograph shape and dynamics) rather than absolute geographic elevation, substantially simplifying the learning problem and improving model convergence.

Deep Learning Architecture and Custom Loss Function

The core model architecture is a feed-forward neural network comprising multiple dense layers (DNN) with Exponential Linear Unit (ELU) activations. Unlike rectified linear unit (ReLU) activations, ELU functions permit negative output values and provide smooth gradients for negative inputs, which is particularly advantageous for learning the non-linear mapping from meteorological forcing variables, characterized by rapid positive transients during storm events, to hydrological responses that include recessions and baseflow conditions below the seasonal mean. To enforce physical consistency in the predictions, the final output layer employs a ReLU activation function, thereby constraining the model outputs to non-negative

values. This design choice ensures that the predicted hydrological variables remain within physically plausible bounds.

Standard regression loss functions such as mean squared error (MSE) penalize large errors quadratically, which often causes the model to over-smooth hydrological peaks and troughs in order to minimize the population-mean error. To prevent this and to ensure the model captures the full amplitude and timing of seasonal hydrographs, the framework employs a custom loss function (designated customLoss1) based on the Index of Agreement (IOA)[20–22]:

$$\text{Loss} = -[\, 1 - \Sigma(o - p)^2 \,/\, \Sigma(|p - \bar{o}| + |o - \bar{o}|)^2 \,]$$

where o represents observed WSE values, p represents model predictions, and $\bar{o}$ is the temporal mean of the observations at a given station. By maximizing the IOA (minimizing its negative), the optimizer is directed to minimize the ratio of the actual prediction error to the potential error, the maximum possible error given the observed variance. This formulation is less sensitive to isolated outliers than MSE and is more representative of model skill in reproducing seasonal variability, making it scientifically superior for hydrological time series applications.

Training Strategy: Cross-Validation and Ensemble Aggregation

To ensure the framework generalizes across the extreme heterogeneity of global river basins ranging from humid tropical rivers with large seasonal amplitudes to arid or regulated systems with muted WSE signals a 10-fold cross-validation strategy was implemented at the station level.

The 9,184 qualifying river reaches were partitioned into 10 approximately equal folds. In each fold, the model was trained on nine folds and validated on the withheld tenth fold, ensuring that every station served as an independent validation target exactly once. This station-level partitioning is critical: it guarantees that the IOA agreement captured during training is not station-specific overfitting but reflects genuine generalization to unseen river locations and hydrological regimes.

The cross-validation procedure generated tenfold-specific daily WSE prediction series (D0 through D9), each representing an independently trained model's estimate for the withheld stations in that fold. These ten predictions were subsequently combined through a secondary stacked ensemble model that ingests D0–D9 alongside the original feature set to produce a stabilized daily WSE estimate (referred to as EST or D2_est2 in the output files, and D_step2_en1 in the source code). Ensemble aggregation suppresses fold-specific noise and reduces prediction variance, particularly during periods with sparse altimetry constraints.

The final densified WSE output is converted back to absolute orthometric height by reversing the normalization applied during preprocessing:

D_step2_en1 = EST + min_ortho_height

This yields a daily WSE value referenced to the global EGM2008 geoid, consistent with the reference frame of the input Hydroweb observations.

Global Dataset Production

The full production pipeline was implemented in Python, with the neural network components developed in TensorFlow/Keras. Following the cross-validation training procedure, the stacked ensemble was applied globally to all 9,184 qualifying reaches to generate continuous daily WSE estimates from January 1, 2008, through May 31, 2025, a total of 6,360 days per reach. GLDAS forcing data were retrieved and pre-processed at the reach level by extracting the GLDAS grid cell values nearest to each SWORD reach centroid. Static RiverAtlas attributes were merged at the reach level using the SWORD reach identifier as the join key.

Data Records

The dataset is archived and publicly accessible at the following Zenodo repository: https://doi.org/10.5281/zenodo.19668644.

Spatial and Temporal Coverage

The dataset provides global coverage constrained by the availability of coincident Hydroweb virtual station observations within the SWORD v16 reach network. Spatial and temporal coverage is summarized as follows:

- Latitude range: −51.9° to 75.3° N
- Longitude range: −177.9° to 179.7° E
- Temporal range: January 1, 2008, to May 31, 2025
- Record duration: median 6,360 days (~17.4 years) per reach
- Number of reaches: 9,184

Coverage is densest in the major river systems of the Amazon, Congo, Nile, Ganges-Brahmaputra, Yangtze, Mississippi, and Danube basins, consistent with the historical distribution of legacy altimetry virtual stations (Figure 2).

Technical Validation

Validation of the dataset was conducted through two complementary approaches: (1) internal 10-fold cross-validation against withheld Hydroweb observations, in which each of the 9,184 reaches served as an independent validation target exactly once; and (2) external, independent validation against SWOT Level-2 river reach observations from the nominal science phase (August 2023 onwards), which represent measurements from a sensor entirely absent from the training data. Performance was assessed using the Pearson correlation coefficient (R), mean bias (model minus observation), mean absolute error (MAE), and the Kling-Gupta Efficiency (KGE) and its decomposed components.

Global Statistical Evaluation

Table 2 summarizes the distribution of validation performance metrics across all stations using percentile-based statistics. The Hydroweb comparison exhibits a median correlation of 0.46, with an interquartile range (IQR) spanning 0.19 to 0.69, indicating moderate but consistent performance across the global network. In contrast, the SWOT comparison yields a higher median correlation (0.62), reflecting improved typical agreement with independently observed WSE dynamics. However, this improvement is accompanied by substantially greater variability, as indicated by a 10th percentile of −0.69, highlighting the presence of poorly performing stations despite strong performance at the upper end (P90 = 0.98).

Bias statistics reveal that the model is effectively unbiased with respect to the Hydroweb calibration dataset (median = 0.00 m), confirming that the cross-validation framework successfully prevents systematic drift. In contrast, the SWOT comparison exhibits a positive median bias of 0.23 m, potentially attributable to differences in measurement physics and residual spatial sampling mismatches between nadir altimetry-based virtual stations and SWOT KaRIn-derived node measurements, despite both datasets being referenced to a common geoid (EGM2008).

Error magnitude, as measured by root mean squared error (RMSE), is broadly comparable between the two datasets, with median values of 0.92 m (Hydroweb) and 0.98 m (SWOT). However, the SWOT distribution shows a heavier upper tail (P90 = 2.58 m), indicating that a subset of reaches experiences larger errors under independent validation conditions.

To provide a more interpretable measure of model skill, the fraction of stations meeting predefined performance thresholds was also evaluated. These thresholds were selected to represent practically meaningful levels of performance for large-scale hydrological applications and are consistent with commonly used interpretative ranges in hydrological modelling literature, where moderate model skill is often associated with efficiency or correlation values on the order of 0.5. Specifically, thresholds were defined as correlation coefficient $R>0.5$, absolute bias $|Bias|<0.5$ m, and $RMSE<1$m. While such thresholds are inherently application-dependent and empirical, they provide a useful benchmark for distinguishing acceptable from poor model performance at global scale.

Under these criteria, approximately 55.5% of stations achieve $R>0.5$ against SWOT observations, compared to 45.4% for Hydroweb. Conversely, 59% of stations exhibit $|Bias|<0.5$m for Hydroweb, compared to 41.2% for SWOT, indicating more consistent bias performance relative to the calibration dataset. Similarly, 56.0% (Hydroweb) and 51.5% (SWOT) of stations achieve RMSE values below 1 m.

Overall, these results indicate that while validation against SWOT yields higher median correlation and improved representation of hydrological variability, it is associated with increased dispersion and reduced robustness across stations, reflecting the greater independence of the SWOT observations from training observations.

Table 2: Distribution of validation performance metrics across all stations, reported at the 10th, 25th, 50th (median), 75th, and 90th percentiles. Additional threshold-based statistics (e.g., fraction of stations with R > 0.5) are discussed in the text.

Metric	Source	P10	P25	P50	P75	P90
R (Correlation)	Hydroweb	-0.01	0.19	0.46	0.69	0.83
	SWOT	-0.69	−0.07	0.62	0.90	0.98
Bias (m)	Hydroweb	−0.86	−0.40	0.00	0.40	0.90
	SWOT	−1.11	−0.36	0.23	0.77	1.52
MAE (m)	Hydroweb	0.48	0.64	0.92	1.37	2.05
	SWOT	0.40	0.63	0.98	1.59	2.58

Bias Assessment

Figure 3 presents the distribution of mean WSE bias across all validation reaches for comparisons against Hydroweb (left panel) and SWOT (right panel). Against the Hydroweb calibration dataset, the model exhibits a near-zero median bias (0.00 m) with a mean of 0.02 m, confirming that the 10-fold training procedure introduces no systematic over- or underestimation at the population level. The distribution is approximately symmetric and unimodal, with the majority of reaches showing biases within ±0.5 m. Against independent SWOT observations, the model exhibits a slightly larger positive median bias of 0.23 m (mean 0.17 m), consistent with known datum differences between the Hydroweb processing chain and the SWOT L2 geoid reference, as well as spatial averaging scale discrepancies between point virtual stations and interferometric reach averages.

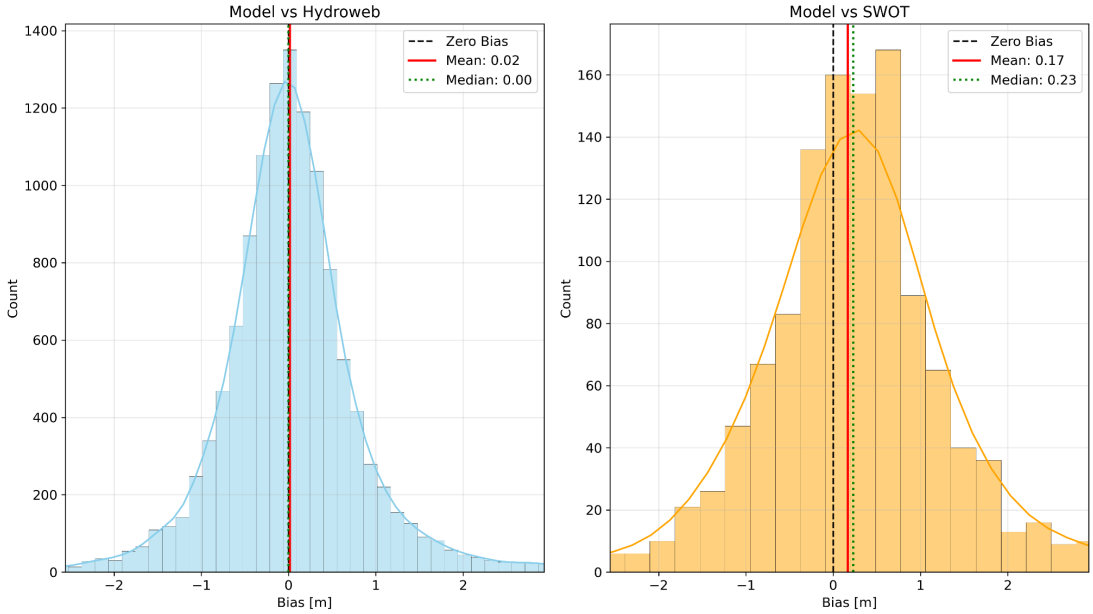

Figure 3: Distribution of mean bias (model minus observation) across validation reaches for comparisons against Hydroweb (left, blue) and SWOT (right, orange). Dashed black line: zero-bias reference; red line: mean bias; green dotted line: median bias. Near-zero Hydroweb bias (mean = 0.02 m, median = 0.00 m) confirms effective bias control during cross-validation training.

Correlation Analysis

Figure 4 shows the cumulative distribution function (CDF) of the Pearson correlation coefficient R across all validation reaches. The median R against SWOT is 0.62, while the median against Hydroweb is 0.46. The top 25% of reaches achieve R > 0.69 against Hydroweb and R > 0.90 against SWOT, indicating strong predictive capability across a substantial fraction of the global network. The higher median R against SWOT relative to Hydroweb is consistent with the model being optimized against the full amplitude of seasonal variability that is better resolved at the reach scale by SWOT than by point virtual stations.

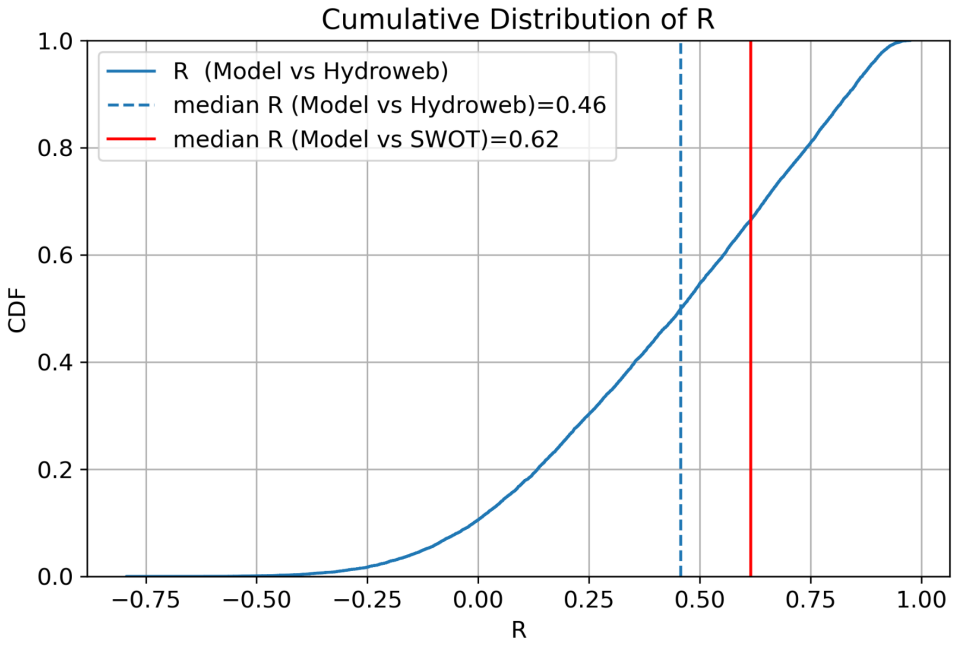

Figure 4: Cumulative distribution function (CDF) of the Pearson correlation coefficient R across all validation reaches. Blue curve: model versus Hydroweb (median R = 0.46, dashed blue line); red vertical line: median R for model versus SWOT (0.62). A substantial fraction of reaches achieves R > 0.75, indicating strong temporal agreement.

Spatial Performance Distribution

Figures 5, 6, and 7 present the global spatial distributions of KGE, R, and VarRatio respectively. The KGE spatial map (Figure 5) reveals broadly positive performance across the major basins of South America, sub-Saharan Africa, and South and Southeast Asia, where strong GLDAS-WSE coupling (driven by large seasonal rainfall signals) produces high model fidelity. Lower performance (KGE Q1, blue) is concentrated in high-latitude North America and Central Asia, where ephemeral rivers, anthropogenic regulation, and ice contamination of altimetry observations degrade both training data quality and the GLDAS-WSE predictive relationship.

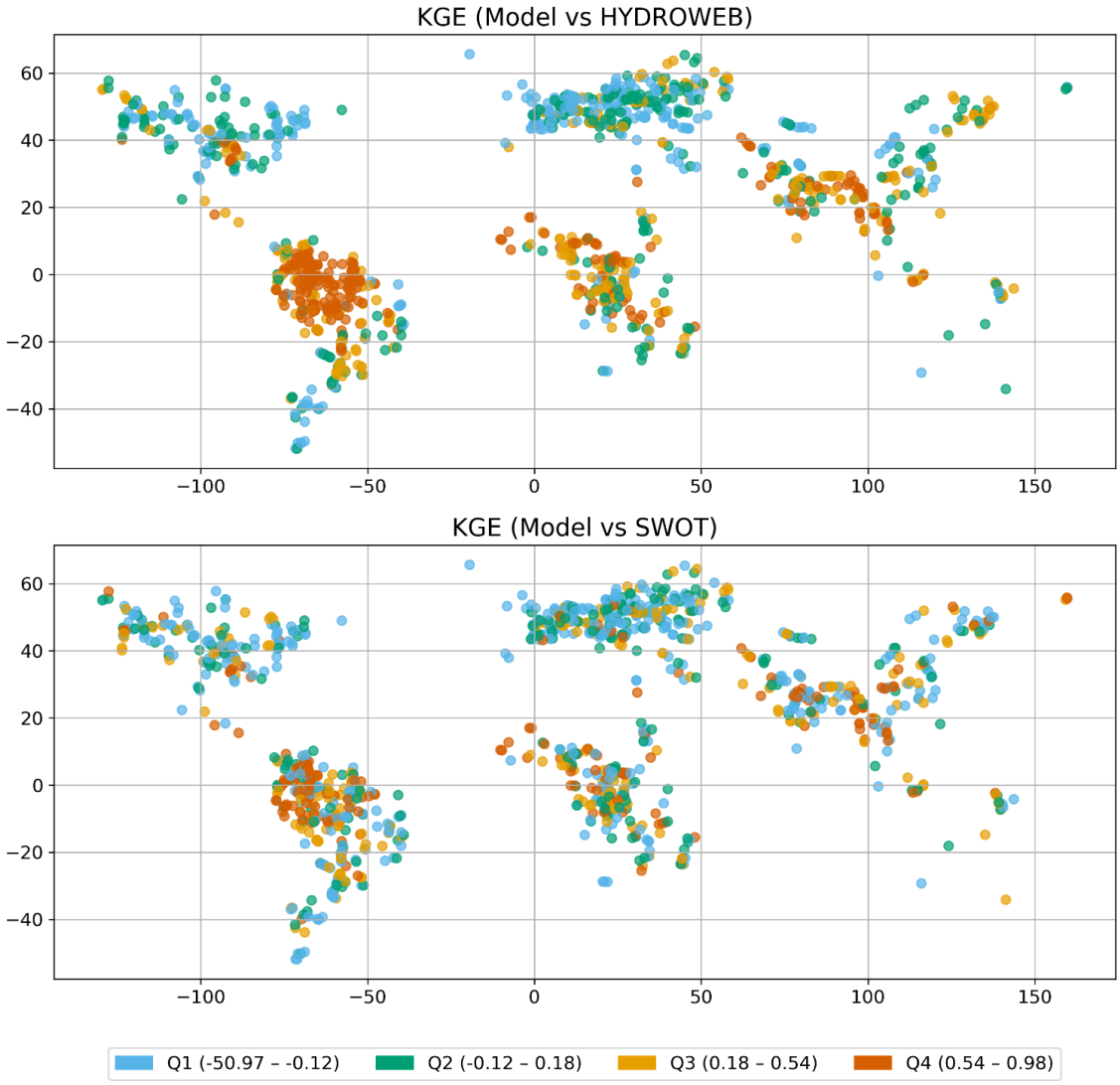

Figure 5: Global spatial distribution of KGE for model comparisons against Hydroweb (left) and SWOT (right), color-coded by quartile (Q1: −50.97 to −0.12; Q2: −0.12 to 0.18; Q3: 0.18 to 0.54; Q4: 0.54 to 0.98). Performance is generally higher in humid tropical and mid-latitude basins where GLDAS meteorological forcing is well coupled to WSE variability.

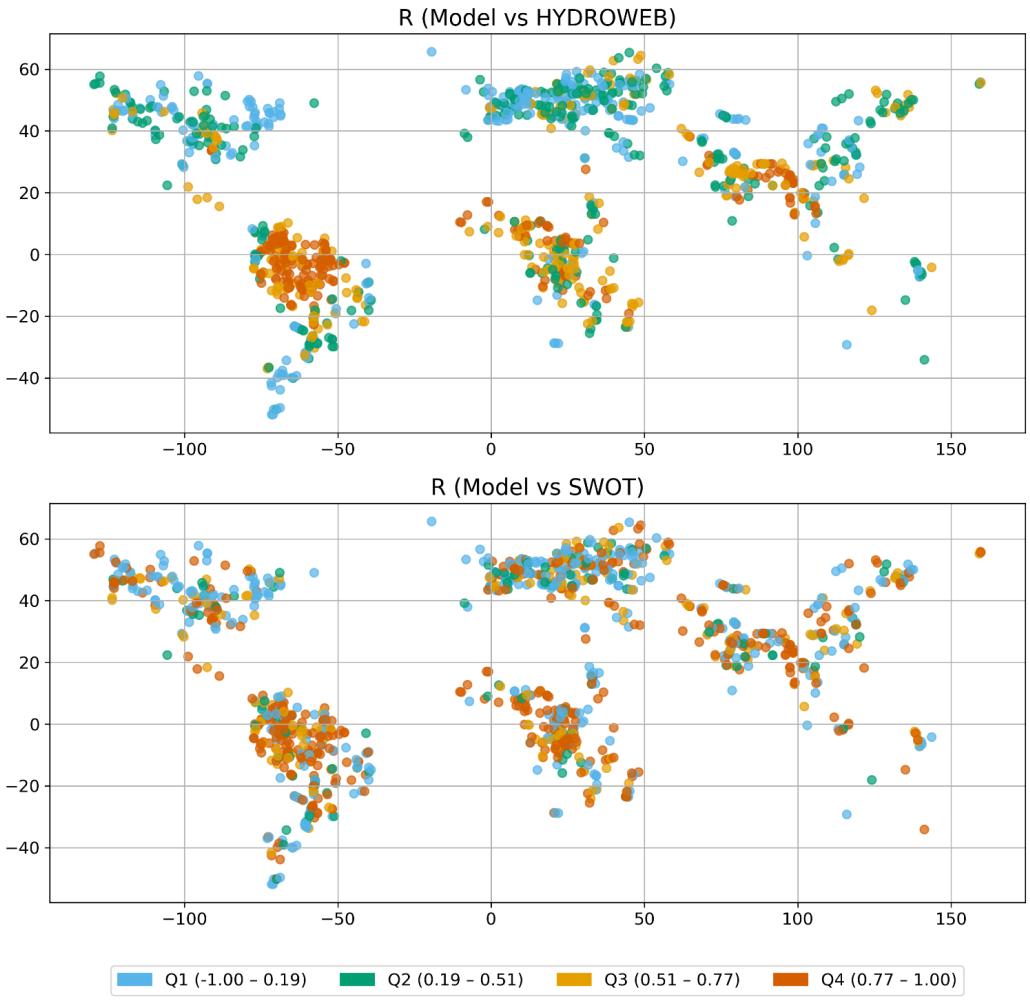

Figure 6: Global spatial distribution of R for model comparisons against Hydroweb (left) and SWOT (right). Quartile ranges: Q1 (−1.00 to 0.19), Q2 (0.19 to 0.51), Q3 (0.51 to 0.77), Q4 (0.77 to 1.00).

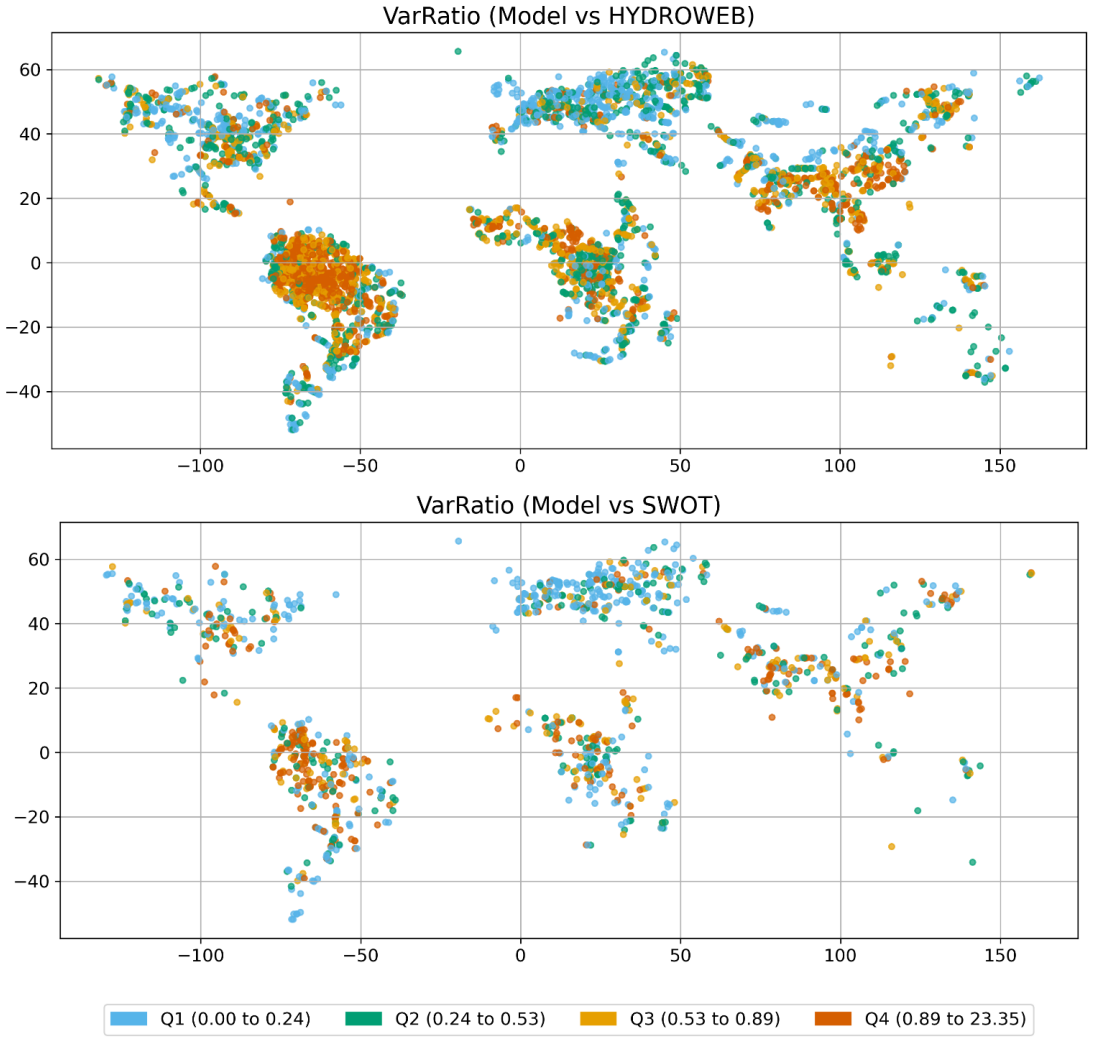

Figure 7: Global spatial distribution of the variance ratio (VarRatio = σ_model / σ_reference) for model comparisons against Hydroweb (left) and SWOT (right). Quartile ranges: Q1 (0.00 to 0.24), Q2 (0.24 to 0.53), Q3 (0.53 to 0.89), Q4 (0.89 to 23.35). Values near unity indicate accurate reproduction of WSE variability amplitude. Values well above 1.0 (extreme Q4 tail) correspond to isolated reaches where the ensemble overestimates variability relative to sparse SWOT observations.

Taylor Diagram Analysis

Taylor diagrams simultaneously summarize normalized standard deviation, Pearson correlation, and centered root mean square error for each validation reach. Figure 8 presents the Taylor diagram for comparisons against Hydroweb; Figure 9 presents the independent SWOT validation diagram. In both cases, the reference point is placed at a normalized standard deviation of 1.0 on the horizontal axis. The distribution of sites in the SWOT Taylor diagram (Figure 9) shows a tighter cluster at correlation values of 0.6–0.9 and normalized standard deviations of 0.6–1.0 compared with the Hydroweb diagram (Figure 8), consistent with the better spatial representativeness of SWOT reach-scale observations relative to point virtual stations.

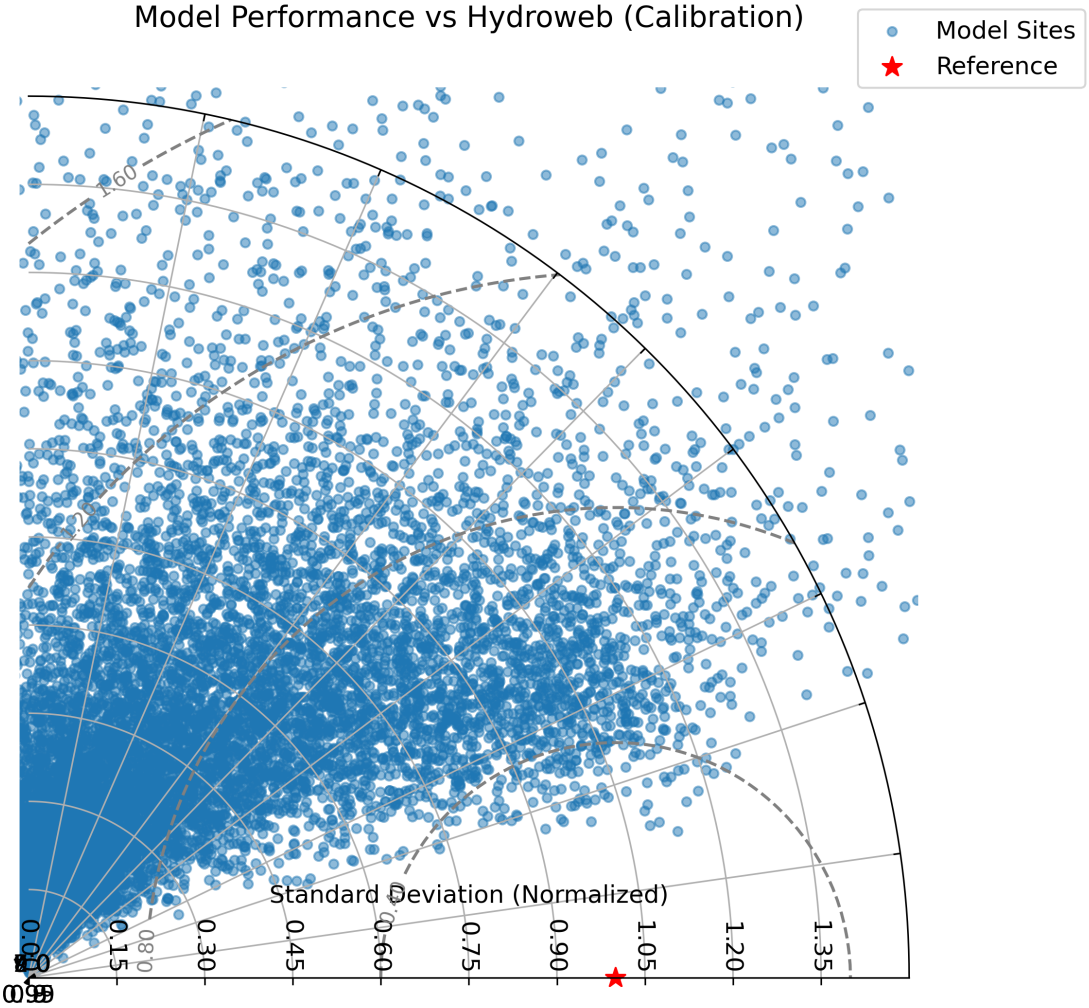

Figure 8. Taylor diagram for model versus Hydroweb calibration comparisons. Each blue point represents one reach. The red star marks the reference (perfect agreement). Angular coordinate = correlation coefficient; radial coordinate = normalized standard deviation; dashed arcs = constant normalized CRMSE.

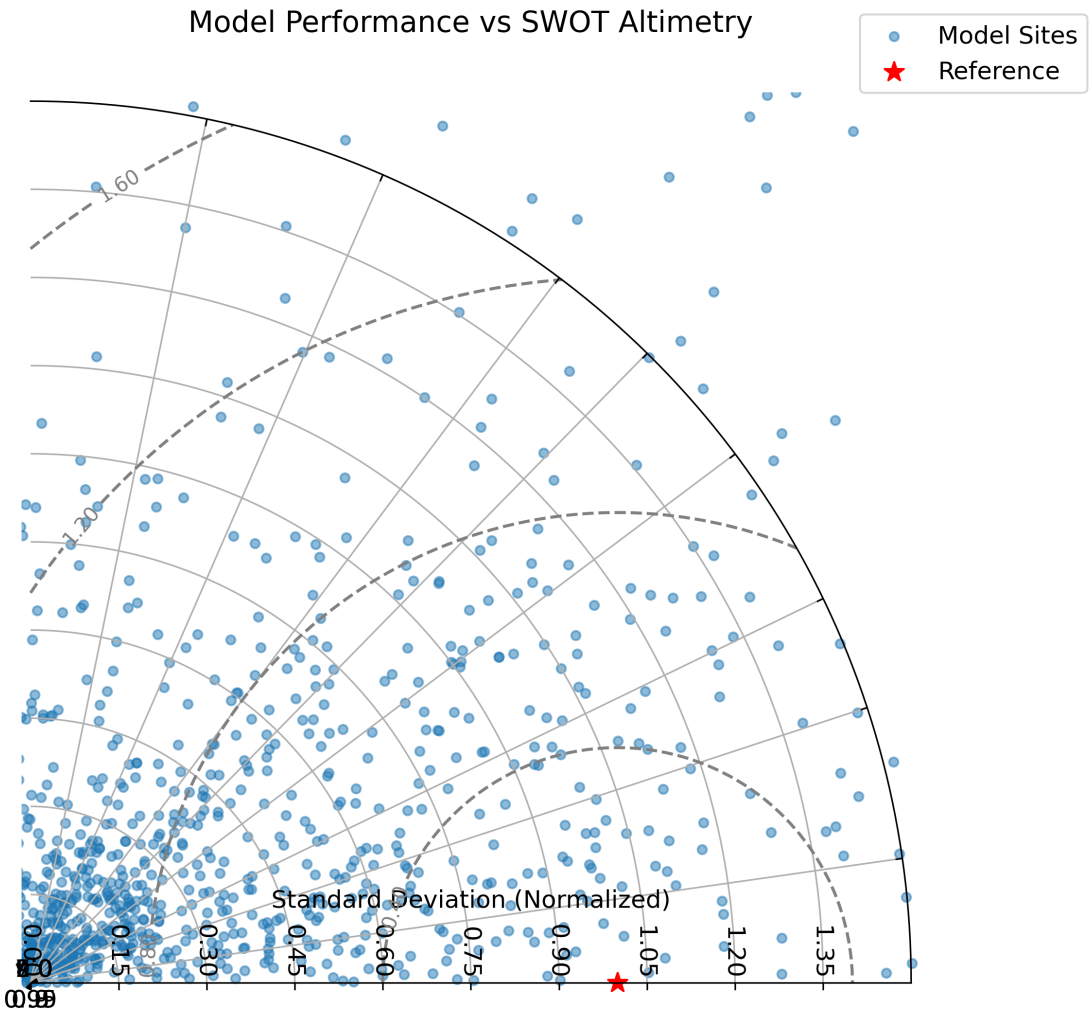

Figure 9. Taylor diagram for model versus independent SWOT observations. The tighter clustering compared with Figure 8 reflects consistent spatial scale between the SWORD-based model output and SWOT reach-averaged measurements.

Error Driver Decomposition

To diagnose the primary sources of KGE degradation at lower-performing reaches, the KGE score was decomposed into its three multiplicative components: correlation (r, timing errors), variability ratio (α = σ_sim/σ_obs, amplitude errors), and bias ratio (β = μ_sim/μ_obs, systematic offset errors). For each reach with KGE in the lowest two quartiles against SWOT, the component contributing most to the KGE deficit was identified as the primary error driver. Figure 10 maps the geographic distribution of primary error drivers, and Figure 11 shows the count of stations in each KGE quartile by error type. Variability errors (amplitude underestimation or overestimation) and correlation errors (timing offsets) account for the overwhelming majority of performance limitations, while bias errors are rare. Variability errors predominate in densely vegetated tropical systems, where radar backscatter noise may contaminate altimetry observations, and in arid regions where ephemeral river dynamics are poorly represented by continuous GLDAS forcing. Timing errors are most prevalent in complex multi-modal flood regimes, such as those found in the semi-arid Sahel and the regulated basins of Central Asia.

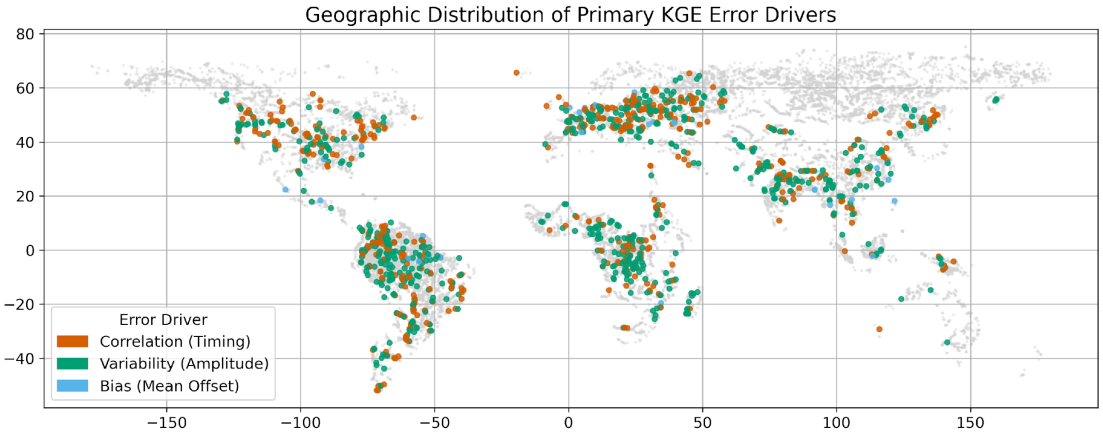

Figure 10. Geographic distribution of primary KGE error drivers at reaches where SWOT-validation KGE falls in Q1 or Q2. Orange: correlation errors (timing); green: variability errors (amplitude); blue: bias errors (mean offset). Gray points: all SWOT-collocated reaches. Variability and timing errors dominate globally, with bias errors confined to a small number of isolated locations.

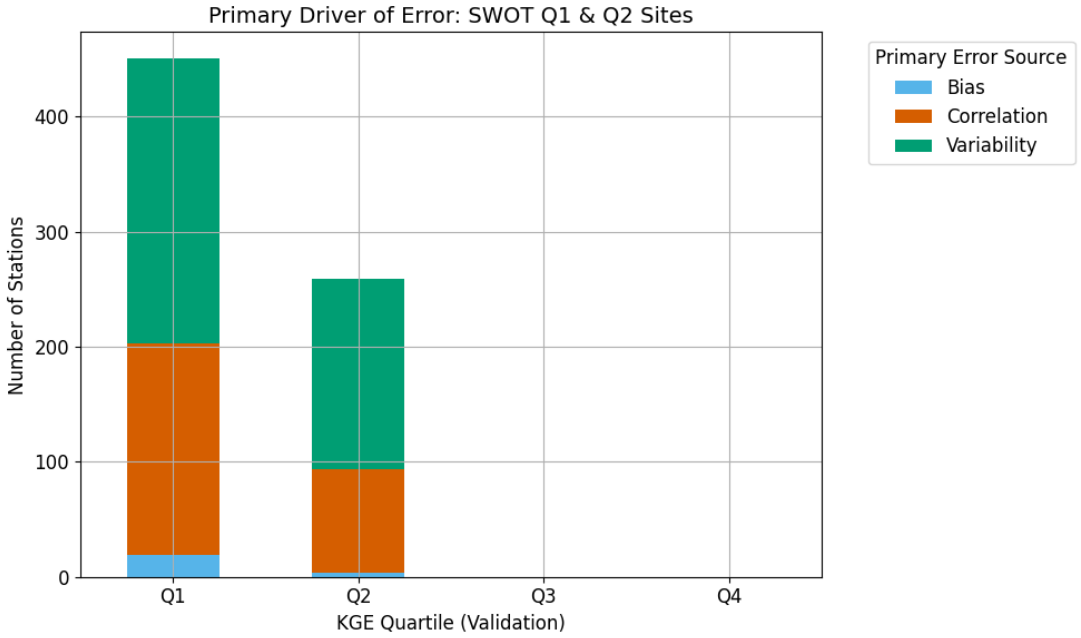

Figure 11. Stacked bar chart showing the count of stations in each SWOT KGE quartile (Q1–Q4) by primary error source: Bias (blue), Correlation (orange), Variability (green). Error driver analysis is applied only to Q1 and Q2 reaches; Q3 and Q4 reaches are not shown. Variability and correlation errors account for the vast majority of low-performance stations.

Hydrograph Fidelity

The example time series shown in Figure 1 (Hydroweb ID 0000000000556) illustrates the model's core capability: the daily ensemble output (D2_est2, blue line) captures high-frequency daily variability driven by GLDAS dynamics that are entirely absent from Hydroweb observations due to their 10–35-day revisit cycles. The model demonstrates high synchronicity with both the baseflow recession limb and the seasonal flood peak, and the independent SWOT observations (green) confirm its accuracy during the SWOT operational period. This

high-frequency reconstruction is the primary added value of the dataset relative to the input altimetry time series.

Uncertainty Considerations

Several sources of uncertainty affect the densified WSE estimates and should be considered by users. First, reaches with fewer valid Hydroweb training observations may exhibit lower accuracy. Second, the median MAE of 0.78 m against Hydroweb (P90 = 1.70 m) indicates that for 90% of global reaches the daily estimation error remains within a range actionable for large-scale hydrological modelling, but local hydraulic modelling requiring sub-decimeter accuracy will require additional site-specific calibration against in-situ gauges. Third, the positive SWOT bias (median 0.23 m) reflects residual datum inconsistencies between the EGM2008-referenced Hydroweb training data and the SWOT geoid processing chain; users requiring absolute WSE accuracy should apply datum corrections at the reach/node level. Fourth, the tenfold-specific predictions D0–D9 provided in the output files may be used to compute per-reach ensemble spread as a proxy for model uncertainty without assuming a specific error distribution.

Data Availability

The dataset is archived and publicly accessible at the following Zenodo repository: https://doi.org/10.5281/zenodo.19668643.

Code Availability

Code will be made publicly available via GitHub repository upon formal acceptance of the manuscript.

Author contributions

All authors contributed equally.

Competing interests

The authors declare that they have no known competing financial interests or personal relationships that could have appeared to influence the work reported in this paper.

Funding

The authors acknowledge funding and programmatic guidance from the NASA EarthRISE. Funding was provided to UAH via the cooperative agreement 80MSFC22N0004 between NASA and UAH.

References

1. Hou, J., van Dijk, A. I. J. M. & Beck, H. E. Global satellite-based river gauging and the influence of river morphology on its application. *Remote Sensing of Environment* **239**, 111629–111629 (2020).

2. Biancamaria, S., Lettenmaier, D. P. & Pavelsky, T. M. The SWOT Mission and Its Capabilities for Land Hydrology. *Surveys in Geophysics* **37**, 307–337 (2016).

3. Crétaux, J. F. *et al.* SOLS: A lake database to monitor in the Near Real Time water level and storage variations from remote sensing data. *Advances in Space Research* **47**, 1497–1507 (2011).
4. Fu, L. L. *et al.* The Surface Water and Ocean Topography Mission: A Breakthrough in Radar Remote Sensing of the Ocean and Land Surface Water. *Geophysical Research Letters* **51**, e2023GL107652-e2023GL107652 (2024).
5. Altenau, E. H. *et al.* The Surface Water and Ocean Topography (SWOT) Mission River Database (SWORD): A Global River Network for Satellite Data Products. *Water Resources Research* **57**, e2021WR030054-e2021WR030054 (2021).
6. Maubant, L., Dodd, L. & Tregoning, P. Assessing the Accuracy of SWOT Measurements of Water Bodies in Australia. *Geophysical Research Letters* **52**, e2024GL114084-e2024GL114084 (2025).
7. Normandin, C. *et al.* First results of the surface water ocean topography (SWOT) observations to rivers elevation profiles in the Cuvette Centrale of the Congo Basin. *Frontiers in Remote Sensing* **5**, 1466695–1466695 (2024).
8. Yu, L., Zhang, H., Gong, W. & Ma, X. Validation of Mainland Water Level Elevation Products From SWOT Satellite. *IEEE Journal of Selected Topics in Applied Earth Observations and Remote Sensing* **17**, 13494–13505 (2024).
9. Patidar, G., Indu, J. & Karmakar, S. Performance Assessment of Surface Water and Ocean Topography (SWOT) Mission for WSE Measurement Across India. *Geophysical Research Letters* **52**, e2025GL115804-e2025GL115804 (2025).
10. Meem, T. H., Rhoads, B. L., Wang, J. & Frasson, R. P. de M. Detecting Water-Surface Superelevation in Meandering Rivers Using Surface Water and Ocean Topography (SWOT) Satellite Data. *Geophysical Research Letters* **53**, e2025GL119167-e2025GL119167 (2026).
11. Andreadis, K. M. *et al.* A First Look at River Discharge Estimation From SWOT Satellite Observations. *Geophysical Research Letters* **52**, e2024GL114185-e2024GL114185 (2025).

12. Getirana, A. *et al.* The SWOT mission will reshape our understanding of the global terrestrial water cycle. *Nature Water 2024 2:12* **2**, 1139–1142 (2024).
13. Halicki, M., Niedzielski, T., Schwatke, C., Scherer, D. & Dettmering, D. Daily river water levels from multi-mission altimetry: A reach-based regression method using the unique SWOT data geometry. *Journal of Hydrology* **673**, 135367–135367 (2026).
14. Paiva, R. C. D., Durand, M. T. & Hossain, F. Spatiotemporal interpolation of discharge across a river network by using synthetic SWOT satellite data. *Water Resources Research* **51**, 430–449 (2015).
15. Li, D., Andreadis, K. M., Margulis, S. A. & Lettenmaier, D. P. A Data Assimilation Framework for Generating Space-Time Continuous Daily SWOT River Discharge Data Products. *Water Resources Research* **56**, e2019WR026999-e2019WR026999 (2020).
16. Larnier, K. *et al.* Estimating Channel Parameters and Discharge at River Network Scale Using Hydrological-Hydraulic Models, SWOT and Multi-Satellite Data. *Water Resources Research* **61**, e2024WR038455-e2024WR038455 (2025).
17. Bonassies, Q. *et al.* Assimilation of SWOT Altimetry Data for Riverine Flood Reanalysis: From Synthetic to Real Data. https://doi.org/10.1109/JSTARS.2026.3659808 (2025) doi:10.1109/JSTARS.2026.3659808.
18. Linke, S. *et al.* Global hydro-environmental sub-basin and river reach characteristics at high spatial resolution. *Scientific Data 2019 6:1* **6**, 283 (2019).
19. Rodell, M. *et al.* The Global Land Data Assimilation System. *Bulletin of the American Meteorological Society* **85**, 381–394 (2004).
20. Willmott, C. J. ON THE VALIDATION OF MODELS. *Physical Geography* **2**, 184–194 (1981).
21. Willmott, C. J. *et al.* Statistics for the evaluation and comparison of models. *Journal of Geophysical Research: Oceans* **90**, 8995–9005 (1985).
22. Sayeed, A. *et al.* A novel CMAQ-CNN hybrid model to forecast hourly surface-ozone concentrations 14 days in advance. *Scientific Reports 2021 11:1* **11**, 10891 (2021).

500